CD47-targeted optical molecular imaging and near-infrared photoimmunotherapy in the detection and treatment of bladder cancer

Yongjun Yang,[1] Xiaoting Yan,[2] Jiawei Li,[2] Chao Liu,[3,5] and Xiaofeng Yang[2,4,5]

[1]Department of Urology, Hunan Provincial People's Hospital, The First Affiliated Hospital of Hunan Normal University, 410005 Changsha, Hunan Province, PR China; [2]First Clinical Medical College, Shanxi Medical University, 030001Taiyuan , Shanxi Province, PR China; [3]Academy of Medical Sciences, Shanxi Medical University, 030001 Taiyuan, Shanxi Province, PR China; [4]Department of Urology, First Hospital of Shanxi Medical University, 030001 Taiyuan, Shanxi Province, PR China

Transurethral resection of bladder tumor (TURBT) followed by intravesical therapy remains the most effective strategy for the management of non-muscle-invasive bladder cancer worldwide. TURBT has two purposes: to remove all visible tumors and to obtain tumor specimens for histopathological analysis. However, the detection of flat and small malignant lesions under white-light cystoscopy is extremely challenging, and residual lesions are still the main reason for the high recurrence rate of bladder cancer. We hypothesized that visual enhancement of malignant lesions using targeted optical molecular imaging could potentially highlight residual tumors in the bladder during surgery, and near-infrared photoimmunotherapy (NIR-PIT) could kill exfoliated cancer cells and residual tumors. A mouse model of complete or partial bladder tumor resection was established under the guidance of optical molecular imaging mediated by indocyanine green and anti-CD47-Alexa Fluor 790, respectively. Once the tumor recurred, mouse model received repeated CD47-targeted NIR-PIT. After complete resection, there was no tumor recurrence. Furthermore, the growth rate of recurrent tumor decreased significantly after repeated NIR-PIT. Therefore, CD47-targeted optical molecular imaging can potentially assist urologists to detect and remove all tumors, and repeated NIR-PIT shows the potential to reduce tumor recurrence rates and inhibit the growth of recurrent tumor.

INTRODUCTION

About 75% of newly diagnosed bladder cancer (BC) manifests as early-stage (Tis, Ta, and T1) lesions confined to the mucosa or submucosa, known as non-muscle-invasive bladder cancer (NMIBC).[1] Transurethral resection of bladder tumor (TURBT) is pivotal in the diagnosis and treatment of NMIBC. Unfortunately, during repeated transurethral resection (reTUR), residual tumors were detected in 17%–67% of Ta patients and 20%–71% of T1 patients, and most of the residual tumors (36%–86%) were located at the initial resection site.[2] The high incidence of residual tumors reflected incomplete bladder tumor resection at the first operation. During the follow-up period, the 5-year recurrence-free survival rates of low-, intermediate-, and high-risk NMIBC were 43%, 33%, and 23%, respectively, and 21% of high-risk NMIBC patients progressed to muscle-invasive bladder cancer (MIBC).[3,4] For NMIBC patients who progressed to MIBC, the 4-year cancer-specific survival rate was only 35%, and the prognosis was worse than that of patients with newly diagnosed MIBC who received radical cystectomy (RC) immediately.[5] Tumor recurrence and progression not only endangers the life span of patients but also has double adverse effects on medical expenses and quality of life due to repeated surgical intervention, which has attracted more and more attention among urologists in recent years.[6,7] Thus, optimizing detection and complete resection of early-stage BC are critical for prolonging overall survival and reducing medical costs.

During white-light cystoscopy (WLC)-assisted transurethral resection, urologists mainly rely on their own clinical experience and indirect visual feedback to determine the location and number of tumor lesions, and the boundary and depth of tumor invasion. Flat and small malignant lesions, particularly carcinoma *in situ* (CIS), are not easily displayed and diagnosed in the bladder wall, based on the feedback of visible images. CIS is a type of high-risk NMIBC that is confined to the mucosa, which can be easily confused with inflammatory lesions due to their similar structural appearance under WLC. Other imaging technologies commonly used in the diagnosis of BC, such as ultrasound, computed tomography (CT), and magnetic resonance imaging (MRI), are mainly used for preoperative diagnosis and postoperative follow-up because they can not conveniently and accurately provide real-time dynamic-imaging information during transurethral resection. In recent years, urologists have begun to use enhanced-imaging technology for surgical navigation.

The latest European Association of Urology (EAU) guidelines on NMIBC recommend that photodynamic diagnosis (PDD) or narrow-band imaging (NBI) can be served as an auxiliary imaging mode of WLC in the process of tumor biopsy and resection.[1] After intravesical instillation of 5-aminolaevulinic acid or hexaminolaevulinic acid, PDD is performed under violet light to improve the detection rate of malignant lesions, especially flat lesions and CIS, and then reduce the risk of tumor recurrence after transurethral resection.[8] NBI is another enhanced-imaging technology, which uses output light with two bandwidths of 415 and 540 nm. These two bandwidths of light can be strongly absorbed by hemoglobin, thus increasing the contrast between normal mucosa and hypervascular malignant lesion areas without intravesical instillation of a photosensitizer in advance. In a multicenter randomized trial, compared with WLC-assisted TURBT, NBI-assisted TURBT showed the ability to increase the tumor detection rate and reduce the recurrence rate of low-risk NMIBC patients.[9] However, the deficiency of PDD and NBI in the detection of BC is that the incidence of false-positive results will increase when inflammatory lesions, scar hyperplasia, and acute bleeding occur in the bladder.[10]

In recent years, in order to improve the specificity and sensitivity of malignant lesion detection, the conventional imaging mode based on functional and structural changes has gradually shifted to molecular imaging based on cellular and molecular pathological processes.[10] Unlike ultrasound or MRI molecular imaging, optical molecular imaging can provide real-time dynamic images during surgery and can be applied to many aspects of cancer surgery, such as detecting small and flat malignant lesions, evaluating the boundary and depth of tumor invasion, and highlighting vital anatomical structures.[11] CD47 is overexpressed in more than 80% of bladder tumor cells but not in normal urothelial cells.[12] Once CD47 binds to signal regulatory protein-α (SIRPα) on phagocytes, the phagocytosis of tumor cells by macrophages is inhibited, thereby promoting tumor proliferation, progression, and metastasis.[13] CD47 has been proved to be a potential target for optical molecular imaging in the detection of BC.[14] The safety and efficacy of CD47-targeted therapy have been explored and verified in clinical trials of various hematological malignancies (ClinicalTrials.gov NCT02663518) and solid cancers (ClinicalTrials.gov NCT02216409).[15,16]

In this study, we hypothesized that CD47-targeted optical molecular imaging could be used to guide real-time bladder tumor resection and that near-infrared photoimmunotherapy (NIR-PIT) could inhibit the growth rate of recurrent tumor. On the basis of the specific binding of CD47 antibody to bladder tumor tissue, we established a novel partial or complete tumor resection model guided by optical molecular imaging, and then we recorded the tumor recurrence rate to test the clinical value of CD47-targeted optical molecular imaging in surgical navigation. Then, we explored the safety and efficacy of CD47-targeted NIR-PIT in xenograft mouse models with residual disease or tumor recurrence *in vivo*. Finally, we tested the diagnostic accuracy of CD47-targeted optical molecular imaging in detecting malignant lesions *in vivo* in an orthotopic rat model of BC.

RESULTS

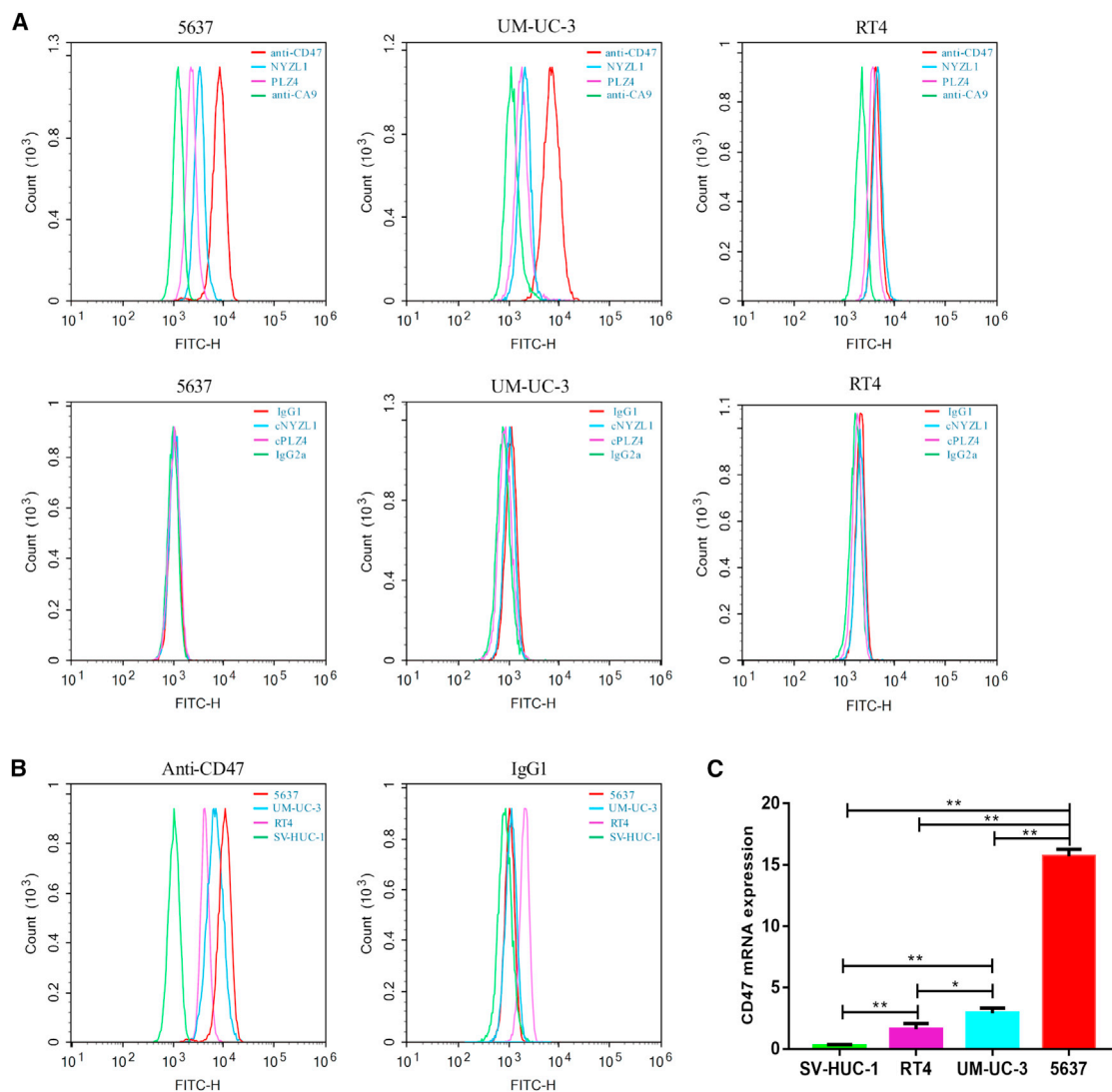### The ability of different molecular tracers to identify human BC cells

To investigate the ability of different molecular tracers to identify human BC cells, cells were incubated with molecular tracers and then analyzed using flow cytometry. The ability of isotype control antibodies or negative control peptides to identify cancer cell lines is weak, whereas the molecular tracers (antibodies and peptides) have a significantly high ability to identify cancer cell lines (Figure 1A). For 5637 cells and UM-UC-3 cells compared with CA9 antibody NYZL1 and PLZ4 molecular tracers, the ability of CD47 antibody to identify BC cell lines is increased. And for RT4 cells compared with CD47 antibody NYZL1 and PLZ4 molecular tracers, the ability of CA9 antibody to identify BC cell lines is reduced.

Human BC cell lines express higher levels of CD47 than SV-HUC-1 cells

To determine whether the expression of CD47 in BC cells is higher than that in human normal urothelial cell line, cancer cells or SV-HUC-1 cells were incubated with anti-CD47-FITC and its isotype control antibody IgG1-FITC and then detected using flow cytometry. The results showed that a high level of CD47 was expressed in BC cells but the level of CD47 was almost undetectable in SV-HUC-1 cells (Figure 1B). As controls, the ability of IgG1 to identify BC cells is non-specific. Therefore, although the CD47 mRNA expression in cancer cell lines and normal urothelial cell line is different, the curves look very similar (Figures 1B and 1C). The expression of CD47 mRNA in human BC cell lines or normal urothelial cell line was also analyzed. The results showed that, compared with SV-HUC-1 cells, the expression of CD47 mRNA in BC cells was significantly higher (5637 versus SV-HUC-1, $p < 0.0001$; UM-UC-3 versus SV-HUC-1, $p = 0.0004$; RT4 versus SV-HUC-1, $p = 0.0065$), which supported the results of flow cytometry (Figure 1C). Among the three types of BC cell lines, 5637 cells had the highest expression level of CD47 mRNA (5637 versus UM-UC-3, $p < 0.0001$; 5637 versus RT4, $p < 0.0001$).

In vitro NIR-PIT of human BC cell lines

We first evaluated CD47-targeted NIR-PIT in three human BC cell lines that express different levels of CD47: 5637, UM-UC-3, and RT4. Cells were incubated with anti-CD47-Alexa Fluor 790 (anti-CD47-AF790) and then exposed to increasing NIR light doses (0–32 J/cm^2) to induce PIT. To measure the direct toxicity of NIR-PIT on cancer cells, propidium iodide staining and flow cytometry were used to detect the fraction of death cancer cells. Cells incubated with PBS and cells without irradiation were used as controls. In cancer cell lines, CD47-targeted NIR-PIT resulted in increased cell death in a light-dose-dependent manner. Significant cancer cells death started at 4 J/cm^2 in 5637 cells, 8 J/cm^2 in UM-UC-3 cells, and 8 J/cm^2 in RT4 cells, and the fraction of cell death increased with the increase of NIR light energy. At the maximum NIR irradiation level of 32 J/cm^2, over 80% of 5637 and UM-UC-3 cells and over 50% of RT4 cells died (Figure 2A).

Figure 1. The ability of molecular tracers to identify BC cell lines, and the expression of CD47 in BC cell lines

(A) The ability of isotype control antibodies or negative control peptides to identify cancer cell lines is weak, whereas the molecular tracers (antibodies and peptides) have significantly high ability to identify cancer cell lines. (B) Compared with normal urothelial cell line SV-HUC-1, the ability of CD47 antibody to identify BC cell lines (5637, UM-UC-3, and RT4) is increased. (C) Compared with SV-HUC-1 cells, the expression of CD47 mRNA in cancer cells was significantly higher (5637 versus SV-HUC-1, p < 0.0001; UM-UC-3 versus SV-HUC-1, p = 0.0004; RT4 versus SV-HUC-1, p = 0.0065), which supported the results of flow cytometry. Among the three types of BC cell lines, 5637 cells have the highest expression level of CD47 mRNA (5637 versus UM-UC-3, p < 0.0001; 5637 versus RT4, p < 0.0001).

To determine whether blocking CD47-SIRPα with CD47 antibody would activate the "eat me" signal, a phagocytosis assay was performed on human BC cell lines. Compared with cancer cell lines treated with isotype control antibody IgG1, CD47 antibody intervention significantly increased the phagocytosis of cancer cells by macrophages (Figure 2B).

In three BC cell lines, since 5637 cells have the highest expression of CD47 mRNA, we then evaluated the phagocytosis of 5637 cells by macrophages under CD47-targeted NIR-PIT (Figure 2C). The 5637 cells were incubated with PBS or anti-CD47 or anti-CD47-AF790 and then seeded onto 96-well plates pre-cultured with RAW 264.7 macrophages. The mixed cells were exposed to a light dose of 4 J/cm² to induce NIR-PIT. Non-irradiated 5637 cells were used as controls. Compared with the control group, the absorbance of cells incubated with anti-CD47-AF790 was significantly decreased under the light irradiation of 4 J/cm² (p < 0.0001), but this phenomenon was not observed in the PBS or anti-CD47 groups (p = 0.08 and 0.59, respectively). The results showed that CD47-targeted NIR-PIT has the dual function of inducing direct cancer cell death and enhancing phagocytosis.
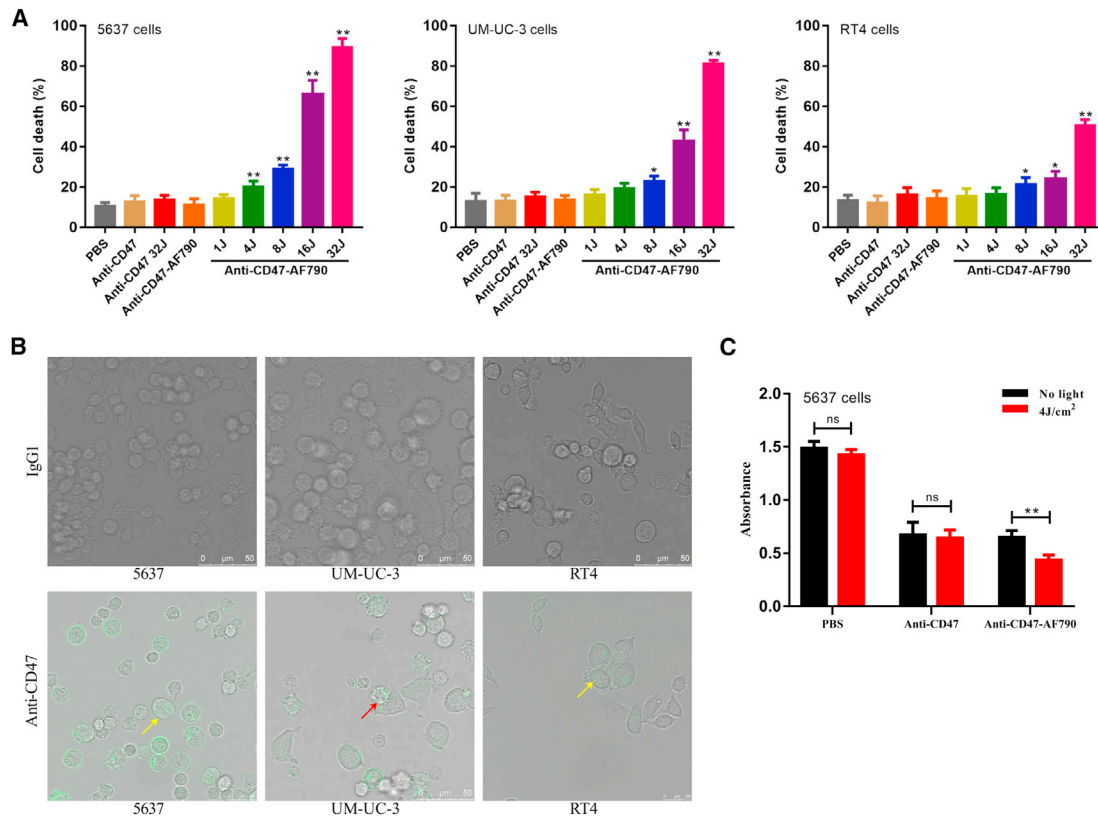
Figure 2. *In vitro* CD47-targeted NIR-PIT for BC cell lines

(A) In BC cell lines, CD47-targeted NIR-PIT resulted in increased cell death in a light-dose-dependent manner. Significant cancer cell death started at 4 J/cm^2 in 5637 cells, 8 J/cm^2 in UM-UC-3 cells, and 8 J/cm^2 in RT4 cells, and the fraction of cell death increased with the increase of NIR light energy. At the maximum NIR irradiation level of 32 J/cm^2, over 80% of 5637 and UM-UC-3 cells and over 50% of RT4 cells died. (B) The arrow (yellow) shows that tumor cells were phagocytized by macrophages; the arrow (red) shows that macrophages were chemotactic and deformed to phagocytize tumor cells. (C) 5637 cells were incubated with PBS or anti-CD47 or anti-CD47-AF790 and then seeded onto 96-well plates pre-cultured with RAW 264.7 macrophages. The cells were exposed to a light dose of 4 J/cm^2 to induce NIR-PIT. Non-irradiated 5637 cells were used as controls. Compared with the control group, the absorbance of 5637 cells incubated with anti-CD47-AF790 was significantly decreased under the light irradiation of 4 J/cm^2 (p < 0.0001), but this phenomenon was not observed in PBS or anti-CD47 groups (p = 0.08 and 0.59, respectively).

Local recurrence occurred in the mouse model with residual tumor after surgery

In order to evaluate the real-time intraoperative guidance value of optical molecular imaging, partial or complete tumor resection was performed on BC xenograft models under CD47-targeted optical molecular imaging. Just as with the procedure of TURBT, two urologists independently determined whether there was residual disease in the wound on the basis of their own clinical experience and visual feedback. The urologists could only accurately point out that 2 of 32 mice with partial tumor resection (groups A, B, D and E) but mistakenly point out that 1 of 16 mice with complete tumor resection (groups C and F) had residual tumors. Thus, visual inspection for residual lesions in the wound had a sensitivity of 6.25% (2/32), a specificity of 93.75% (15/16), a positive predictive value of 66.67% (2/3), and a negative predictive value of 33.33% (15/45).

In the tumor volume measurement of the xenograft mouse model, microCT scanning has been proved to be more accurate than external caliper.[17] Thus, before the surgical wound was closed, we performed microCT scanning in nude mice to evaluate whether there were residual lesions in the wound. The results showed that microCT imaging could not distinguish residual lesions from adjacent normal tissues (Figure 3A).

In groups C and F, the bladder tumor was completely removed under the guidance of optical molecular imaging, and there was no tumor recurrence. In groups A and D, the bladder tumor was partially removed under the guidance of optical molecular imaging, and the tumor recurrence rates were 87.5% (7/8) and 75% (6/8), respectively. In group E, mice received CD47-targeted NIR-PIT immediately and 24 h after surgery, and 50% (4/8) of those mice had tumor recurrence (Figure 3A), while the remaining 50% (4/8) of mice had no tumor recurrence (Figure 3B). In groups A, , and E, the tumor recurrence rate of group E was lower than that of groups A and D, but the difference was not statistically significant (E versus A, p = 0.28; E versus D, p = 0.61).
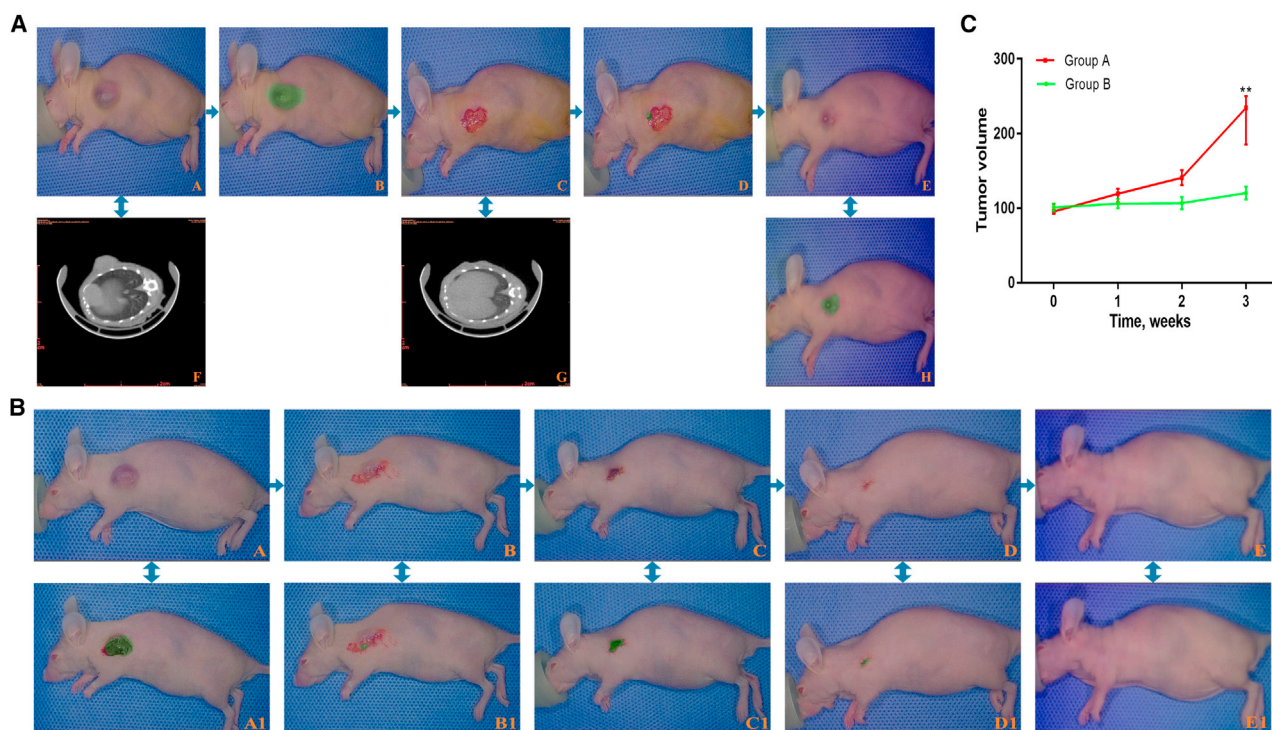
Figure 3. CD47-targeted optical molecular imaging and NIR-PIT for the diagnosis and treatment of residual BC

(A) Tumor recurrence occurred after NIR-PIT in mice with residual disease. (A) Visible image of xenograft mouse model. (B) Under optical molecular imaging, the fluorescent and visible fusion image of xenograft mouse model. (C) Before the wound was closed, visible image of mouse with residual disease. (D) Under optical molecular imaging, the fluorescent and visible fusion image of mouse with residual disease. The tissue with fluorescence signal in the wound represents the residual disease. (E) Visible image of mouse with tumor recurrence. (F) MicroCT image of xenograft mouse model. (G) MicroCT image of mouse with residual disease. (H) Under optical molecular imaging, the fluorescent and visible fusion image of mouse with tumor recurrence. (B) No tumor recurrence occurred after NIR-PIT in mice with residual disease. (A) Visible image of xenograft mouse model. (B) Visible image of mouse with residual disease. (C) One day after NIR-PIT, visible image of mouse with residual disease. (D) Two days after NIR-PIT, visible image of mouse with residual disease. (E) One week after NIR-PIT, visible image of mouse without tumor recurrence. (A1–E1) Under optical molecular imaging, the fluorescent and visible fusion image corresponding to visible image of (A–E). (C) Compared with the control group with no intervention, the tumor growth rate of mice in group B was significantly reduced (p < 0.0001).

Evaluation of the therapeutic effect of repeated CD47-targeted NIR-PIT in the xenograft mouse model with tumor recurrence

To evaluate the therapeutic effect of NIR-PIT, mice with tumor recurrence in group B received repeated CD47-targeted NIR-PIT. In groups A and B, tumor recurrence occurred in seven and eight mice, respectively. Seven mice in group B were randomly selected to receive repeated NIR-PIT, and seven mice with tumor recurrence in group A did not receive any intervention. Compared with the control group with no intervention, the tumor growth rate of mice in group B was significantly lower (p < 0.0001; Figure 3C).
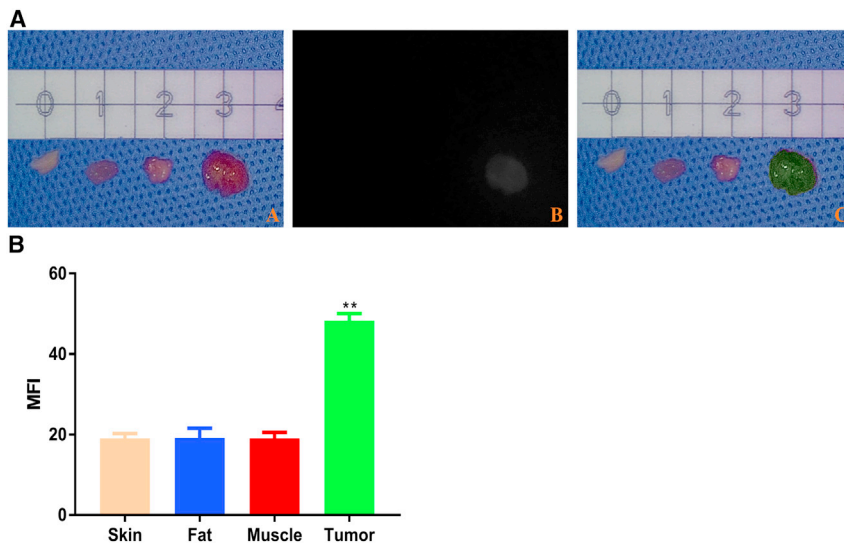
Ex vivo optical molecular imaging of partially resected tumor specimens

In groups D and E, mice underwent partial tumor resection under the guidance of CD47-targeted optical molecular imaging, and then the tumor specimens and adjacent normal tissues (skin, fat, and muscle) were collected for in *ex vivo* optical molecular imaging (Figure 4A). Under optical molecular imaging, the mean fluorescence intensity (MFI) of tumor specimens and adjacent normal tissues (skin, fat,

and muscle) were recorded. The fluorescence signal of tumor specimens was significantly higher than that of adjacent normal tissues (p < 0.0001). On average, the MFI of tumor specimens was about 2.5 times that of adjacent normal tissues (Figure 4B).

In vivo optical molecular imaging in an orthotopic rat model of BC

Two Wistar rats died of other causes before space-occupying lesions were found in the bladder. When space-occupying lesions were confirmed by microMRI scanning, anti-CD47-AF790 molecular tracer was infused into the bladder through the urethra, and then the entire bladder mucosa was imaged using hand-held NIR imaging equipment (Figure 5). During the examination, the bladder mucosa with fluorescence signal was marked, while the space-occupying lesions without fluorescence signal were considered as suspicious malignant lesions. For each rat, when the sum of the fluorescent-labeled sites and the suspicious malignant lesions is less than 5, a random biopsy of bladder mucosa shall be performed to make the total number of specimens not less than 5. Through this procedure, a total of 146

Figure 4. *Ex vivo* optical molecular imaging of partially resected tumor specimens

(A) From left to right, the tissue samples were skin, muscle, fat, and tumor tissue. (A) Visible image of tumor specimen and adjacent normal tissues (skin, fat, and muscle). (B) Fluorescent image of tumor specimen and adjacent normal tissues (skin, fat, and muscle). (C) Fluorescent and visible fusion image of tumor specimen and adjacent normal tissues (skin, fat and muscle). (B) The gray values of MFI of skin, fat, and muscle were 19.00 ± 1.27, 19.17 ± 2.40, and 19.00 ± 1.55, respectively, and there was no significant difference among them (skin versus fat, $p = 0.88$; skin versus muscle, $p = 0.99$; fat versus muscle, $p = 0.89$). The gray value of MFI of tumor specimen was 48.33 ± 1.75, which was significantly higher than that of adjacent normal tissues (skin, fat, and muscle) ($p < 0.0001$). On average, the MFI of tumor specimens was about 2.5 times that of adjacent normal tissues.

tissue specimens were collected, including 87 fluorescent-labeled sites, 12 suspicious malignant lesions, and 47 random biopsies. Histopathological analysis confirmed that 80 of 87 fluorescent-labeled sites, 8 of 12 suspicious malignant lesions, and 3 of 47 random biopsies contained tumor tissue. In other words, among 146 specimens, 91 tumor tissues and 55 normal tissues were confirmed by histopathological analysis. Under CD47-targeted optical molecular imaging, fluorescence signals were detected in 80 tumor tissues, but not in 48 normal tissues. Therefore, the sensitivity and specificity of CD47-targeted optical molecular imaging in the detection of bladder tumor were 87.9% (80/91) and 87.3% (48/55), respectively.

DISCUSSION

According to their molecular size, molecular tracers can be subdivided into the following five classes: monoclonal antibodies, antibody fragments, protein scaffolds, peptides, and small molecules.[18] So far, there is no study to investigate the difference of the ability of different molecular tracers to identify BC cells. By consulting the relevant literature on PubMed, Web of Science, and Scopus, the molecular tracers used in the diagnosis and treatment of BC were summarized and analyzed.[14,19–28] The results showed that the main molecular tracers for bladder tumors were monoclonal antibodies and peptides (Table 1). Epidermal growth factor receptor (EGFR) was overexpressed in 74% of bladder tumor tissues,[29] and was low-expressed in normal transitional epithelium.[30] However, the results of The Cancer Genome Atlas (TCGA) project demonstrated that the amplification rate of EGFR in MIBC was only 11%, which limited it being an effective target for the management of BC.[31] Human epidermal growth factor receptor 2 (HER-2) was overexpressed in about 40% of bladder tumor tissues but not in normal bladder epithelial cells.[30] Immunohistochemical analysis showed that the expression of CA9 in normal urothelial cells was negative but that more than 70% of malignant lesions were positive, and that the expression level of CA9 in Ta stage and low-grade NMIBC was significantly increased.[32] Meanwhile, as a

urine marker, the sensitivity and specificity of CA9 in the diagnosis of BC were 86.2% and 95.1%, respectively, and the prediction accuracy of BC was significantly higher than that of urine exfoliated cytology.[33] CD47 was overexpressed in more than 80% of BC cells, and it was overexpressed in both NMIBC and MIBC but not in normal urothelial cells. The sensitivity and specificity of anti-CD47-Qdot625-mediated optical molecular imaging in the detection of bladder malignant lesions were 82.9% and 90.5%, respectively.[14] Therefore, in this study, we chose CD47 antibody and CA9 antibody as the research objects.

Unlike monoclonal antibodies, the binding site of peptides to BC cells is not clear, so it is impossible to quantitatively analyze the expression level of this site on the cell membrane.[24–27] Thus, NYZL1 and PLZ4 peptides screened by different techniques were selected. NYZL1 peptide was screened by phage display technology, while PLZ4 peptide was screened by the "one bead, one compound" combinatorial chemistry method.

After BC cells were incubated with molecular tracers, the results of flow cytometry showed that, compared with the other three molecular tracers (NYZL1, PLZ4, and CA9 antibodies), the ability of CD47 antibody to identify cancer cells was increased. Meanwhile, compared with normal urothelial cells, the ability of CD47 antibody to identify BC cells was increased, and the expression level of CD47 mRNA in BC cells was significantly higher. And then, we found that in CD47-expressing BC cell lines CD47-targeted NIR-PIT has a direct killing effect on cancer cells in a light-dose-dependent manner. At the maximum light-energy level, the specific cell death rate of 5637 cells with the highest expression of CD47 mRNA induced by NIR-PIT was up to 89.66%.

Urologists mainly rely on clinical experience, endoscopy training, and indirect visual feedback when delineating and resecting bladder malignant lesions. However, determining the boundary and number of
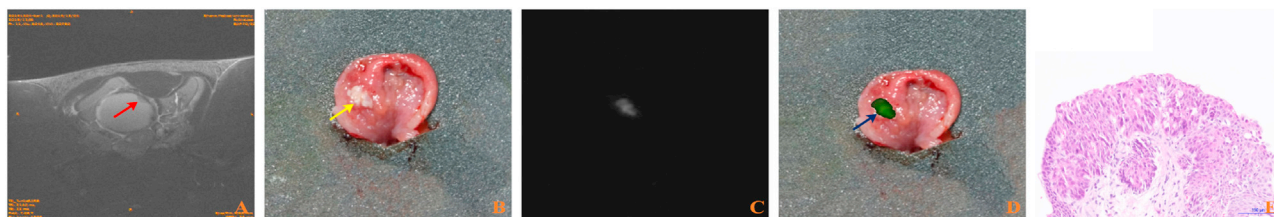
Figure 5. *In vivo* optical molecular imaging in orthotopic rat model of BC

(A) MicroMRI image of bladder in orthotopic rat model of BC. The arrow (red) shows that malignant lesion in the rat bladder. (B) Visible image of bladder in orthotopic rat model of BC. The arrow (yellow) shows that malignant lesion in the rat bladder. (C) Fluorescent image of bladder in orthotopic rat model of BC. (D) The fluorescent and visible fusion image of bladder in orthotopic rat model of BC. The arrow (blue) shows that malignant lesion in the rat bladder. (E) HE staining of tumor specimen.

bladder tumors based on these subjective assessments is challenging and may lead to residual disease, which is the main cause of early tumor recurrence and ultimately affects the oncological prognosis. Complete resection with negative tumor margins must also be balanced with preserving the surrounding structures to minimize the occurrence of bladder perforation. Although the EAU guidelines recommend selective biopsy of the wound after transurethral resection, this procedure can examine only a small part of the tumor base and is prone to sampling errors. A systematic review of the clinical data of 8409 NMIBC patients showed that 17%–67% of patients with stage Ta and 20%–71% of patients with stage T1 had residual tumors at the time of reTUR, and most (36%–86%) of them were located at the initial resection site. Meanwhile, the rates of tumor upstaging in Ta and T1 patients were 0%–8% and 0%–32%, respectively.[7] As a result, the recurrence and progression rates of NMIBC patients were 15%–61% and 0.2%–17% at 1 year, and 31%–78% and 0.8%–45% at 5 years, respectively.[1] Compared with the newly diagnosed stage T2 BC patients who underwent RC immediately, patients with NMIBC upstaged to stage T2, confirmed by histopathological analysis after RC had a worse oncological prognosis.[34]

Several optical-imaging technologies have been developed as an auxiliary mode of WLC to assist urologists in improving intraoperative decision-making. According to the imaging field of view, optical-imaging technology can be subdivided into two modes, namely macroscopic imaging and microscopic imaging. PDD and NBI belong to the macroscopic-imaging mode and examine a wide area of bladder mucosa in a way similar to WLC. Through additional contrast enhancement, suspicious malignant lesions can be highlighted, and then the patient's oncological prognosis is improved.[10] Due to the lack of tumor specificity, although PDD and NBI can improve the detection rate of flat lesions and CIS, the incidence of false-positive results will increase if there are inflammatory lesions, acute bleeding, and previous intravesical therapy in the bladder.[35] Confocal laser endoscopy (CLE) and optical coherence tomography (OCT) are real-time microscopic-imaging modes. Through high-resolution imaging of suspicious malignant lesions, the pathological information about the changes in tissue microstructure and cell morphology can be obtained.[36,37] Unfortunately, only a limited area of bladder mucosa can be examined under the visual field of CLE and OCT. Therefore, the application of microscopic-imaging

mode needs to be combined with an additional, macroscopic-imaging technology (such as WLC, PDD, or NBI) to determine the location of suspicious malignant tissues first.[38]

In this study, we first established a mouse model of complete or partial bladder tumor resection under the real-time guidance of optical molecular imaging. Indocyanine green (ICG) is a non-toxic fluorescent dye that can be administered intravenously and then used for optical molecular imaging, which has been approved by the U.S. Food and Drug Administration. Although ICG lacks tumor specificity, it can accumulate in tumor tissues via the enhanced permeability and retention effect. Thus, under optical molecular imaging mediated by ICG, residual lesions in the surgical wound can be detected after tumor resection.[39] Theoretically, compared with ICG, fluorescent dye-labeled CD47 antibody is a more valuable molecular tracer in the detection of BC due to its tumor specificity. There was no tumor recurrence in the mouse model of complete tumor resection under the real-time guidance of CD47-targeted optical molecular imaging, indicating that CD47-targeted optical molecular imaging has potential navigation value in bladder tumor resection. Meanwhile, CD47-targeted optical molecular imaging has high diagnosis accuracy in the detection of BC in an orthotopic rat model. Then, we evaluated the therapeutic effect of CD47-targeted NIR-PIT in a mouse model with residual bladder tumors. Compared with the mice in group A (no intervention) and group D (immunotherapy alone), the tumor recurrence rate of the mice in group E decreased after NIR-PIT intervention, but the difference was not statistically significant. Similarly to intravesical therapy after TURBT, we will explore whether CD47-targeted NIR-PIT maintenance therapy can significantly reduce the recurrence rate in mice with residual tumor in the future. Finally, the mice that underwent partial tumor resection (group B) received CD47-targeted NIR-PIT maintenance therapy after tumor recurrence, and the tumor growth rate was significantly lower than that of mice without intervention (group A).

Due to its easy access, the urinary tract is very suitable for endoscopic molecular imaging and NIR-PIT. Human bladder is a hollow organ with high compliance, which provides an ideal closed darkroom for endoscopic molecular imaging without the interference of external light sources. In addition to systemic intravenous administration, intravesical instillation provides an alternative route to increase the

Table 1. Comprehensive overview of molecular tracers used in bladder cancer

Tracer type	Compound name	Target	Fluorophore	Application	Study design	Sensitivity	Specificity
Antibodies	CD47 antibody[14]	CD47	Qdot625	Optical molecular imaging	*In vitro*: fresh intact bladder specimen	82.9%	90.5%
	CD47 antibody[19]	CD47	AF790	Optical molecular imaging	*In vitro*: fresh bladder tumor specimen	NA	NA
	CAIX antibody[20]	CAIX	Qdot625	Optical molecular imaging	*In vitro*: fresh intact bladder specimen	88.00%	93.75%
	CD47 antibody[21]	CD47	IR700	NIR-PIT	*In vitro*: bladder tumor cell lines	NA	NA
					In vivo: xenograft mouse model		
	Panitumumab[22]	EGFR	IR700	NIR-PIT	*In vitro*: bladder tumor cell lines	NA	NA
					In vivo: xenograft mouse model		
	Panitumumab	EGFR	IR700	NIR-PIT	*In vitro*: bladder tumor cell lines	NA	NA
	Trastuzumab[23]	HER-2			*In vivo*: xenograft mouse model		
Peptides	CSNRDARRC[24]	NA	Fluorescein	Optical molecular imaging	*In vitro*: human bladder cancer tissue	NA	NA
					In vivo: orthotopic rat model		
	NYZL1[25]	NA	FITC	Optical molecular imaging	*In vitro*: human bladder cancer tissue	NA	NA
					In vivo: xenograft mouse model		
	PLSWT7[26]	NA	IRDye800CW	Optical molecular imaging	*In vivo*: fresh intact bladder specimen	84.0%	86.7%
	PLZ4[27]	NA	Cy5.5	Optical molecular imaging	*In vitro*: bladder tumor cell lines	NA	NA
					In vivo: xenograft mouse model		
	pHLIP[28]	NA	ICG	Optical molecular imaging	*In vitro*: fresh intact bladder specimen	97%	100%[a]

AF790, Alexa Fluor 790; NA, not applicable; IR700, IRDye700DX; NIR-PIT, near-infrared photoimmunotherapy; EGFR, epidermal growth factor receptor; HER-2, human epidermal growth factor receptor-2; FITC, fluorescein isothiocyanate; ICG, indocyanine green.
[a]If necrotic and previously chemotherapy tissues were considered as false positive, the specificity was reduced to 80%.

local concentration of molecular tracers and reduce systemic side effects. Using a NIR cystoscopic camera, the fluorescence signal from fluorescent -dye-labeled molecular tracer would allow for intraoperative optical molecular imaging, thereby helping the urologist to improve the detection rate of flat and small lesions and evaluate the resection margin to reduce recurrence. After transurethral resection, a light-guide bundle is inserted into the bladder through a catheter, and PIT can be induced by direct NIR light irradiation, thereby specifically killing the exfoliated tumor cells and residual diseases. The fresh intact tumor specimens were collected after *en bloc* resection and imaged using a fluorescence camera and a fluorescence microscope, respectively. Through fluorescence images, pathologists can purposefully select tissue samples for histopathological analysis to evaluate the surgical margins and the depth of tumor invasion and then provide urologists with useful information about which patients need to receive reTUR or RC (Figure 6).

In summary, the ability of CD47 antibody to identify BC cell lines is increased compared with the other three molecular tracers (NYZL1, PLZ4, and CA9 antibodies). CD47-targeted optical molecular imaging has high diagnosis accuracy in the detection of BC and has potential navigation value in the resection of BC. CD47-targeted NIR-PIT has a direct killing effect on cancer cells in a light-dose-dependent manner and can inhibit the growth rate of recurrent tumors. The combination of targeted optical molecular imaging and NIR-PIT may meet the needs of special imaging for the detection of all malignant lesions and precise targeted therapy, thus providing a complementary option in the management of BC.

MATERIALS AND METHODS

Reagents

ICG for injection was purchased from Dandong Yichuang Pharmaceutical (Liaoning, China). Anti-CD47, anti-CD47-fluorescin isothiocyanate (anti-CD47-FITC) and its isotype control antibody normal mouse IgG1-FITC, anti-CA9-FITC and its isotype control antibody normal mouse IgG2a-FITC, and anti-CD47-AF790 were purchased from Santa Cruz Biotechnology (Oregon, USA). CSSPIGRHC (NYZL1) peptide and its negative control CRIGSPHSC (cNYZL1) peptide CQDGRMGFC (PLZ4) peptide and its negative control CQAGRMGFC (cPLZ4) peptide were synthesized by Chinese Peptide (Hangzhou, China) using the standard solid-phase fluorenylmethyloxycarbonyl chloride chemistry. All peptides were purified by high-performance liquid chromatography with a minimum purity of 99.0%. The sequence and structure of each peptide were characterized and verified by mass spectrometry. FITC-labeled NYZL1 (NYZL1-FITC), FITC-labeled cNYZL1 (cNYZL1-FITC), FITC-labeled PLZ4 (PLZ4-FITC), and FITC-labeled cPLZ4 (cPLZ4-FITC) were also synthesized in the same manner as above.

Cell lines

RAW 264.7 macrophages, human urothelial cell line SV-HUC-1, and human BC cell lines 5637, UM-UC-3, and RT4 were purchased from the Cell Bank of the Chinese Academy of Sciences (Shanghai, China). All three BC cell lines are derived from male patients, but have different grades and genome instability groups. According to the urothelial BC cell lines index,[40] RT4, 5637, and UM-UC-3 have a low, intermediate, and high genome instability group, respectively. Apart from TERT and
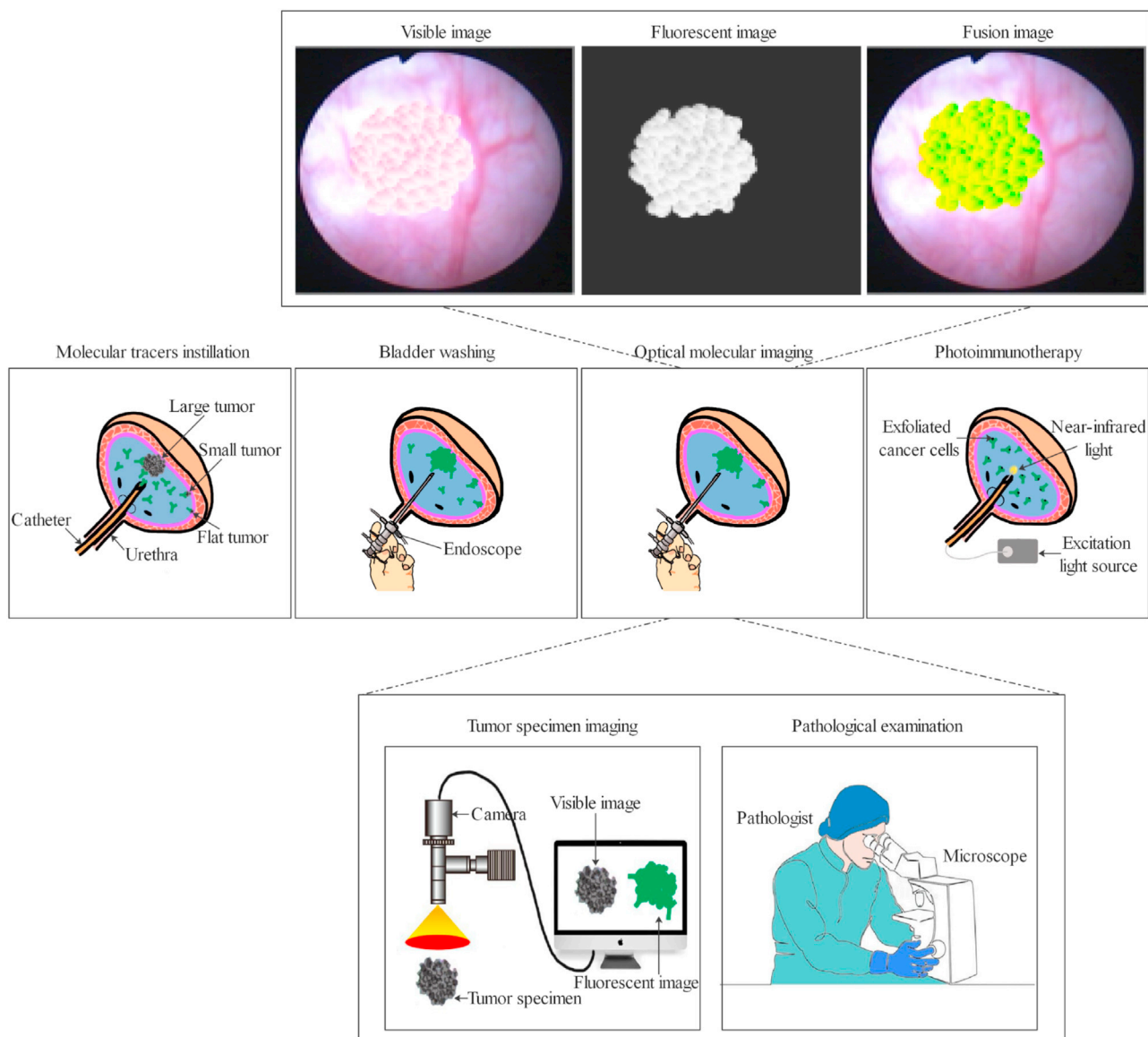
Figure 6. Schematic diagram of targeted optical molecular imaging and NIR-PIT for the management of BC

Using a NIR cystoscopic camera, the fluorescence signal from fluorescent dye would allow for intraoperative optical molecular imaging, thereby helping the urologist to improve the detection of flat and small lesions and evaluate the resection margin to reduce recurrence. After transurethral resection, a light-guide bundle is inserted into the bladder through a catheter, and PIT can be induced by direct NIR light irradiation, thereby specifically killing the exfoliated tumor cells and residual diseases. The fresh intact tumor specimens were collected after *en bloc* resection and imaged using a fluorescence camera and a fluorescence microscope, respectively. Through the fluorescence images, pathologists can purposefully select tissue samples for histopathological analysis to evaluate the surgical margins and the depth of tumor invasionand then provide urologists with useful information about which patients need to undergo reTUR or RC.

TP53 mutations in all three cancer cell lines, additional gene mutations are FGFR3 in RT4 cells and KRAS2 in UM-UC-3 cells. All cell lines were cultured under specific conditions recommended by the official website of the Cell Bank of the Chinese Academy of Sciences.

Flow cytometry
Three BC cell lines were trypsinized from a culture flask and then incubated with molecular tracers and its isotype control antibodies or negative control peptides, respectively. The molecular tracers used in this assay were as follows: anti-CD47-FITC, anti-CA9-FITC, NYZL1-FITC, and PLZ4-FITC. Flow cytometry was performed on the FACSCanto II flow cytometry system (BD Biosciences, USA), and the data were analyzed using FlowJo software. Then, SV-HUC-1 cells were incubated with anti-CD47-FITC, and the expression of CD47 on cell membrane was detected by flow cytometry.

Reverse transcription-quantitative polymerase chain reaction

According to the manufacturer's protocol, TRIzol reagent (Thermo Fisher Scientific) was used to extract total RNA from SV-HUC-1 and three BC cell lines, respectively. The yield of RNA was determined using a spectrophotometer (Thermo Fisher Scientific), and the integrity was evaluated using agarose gel electrophoresis stained with ethidium bromide.

Real-time PCR was performed using LightCycler 480 II Real-time PCR Instrument (Roche, Swiss) with a PCR reaction mixture that included cDNA, 2×PerfectStart Green qPCR SuperMix, forward primer, reverse primer, and nuclease-free water. The expression level of CD47 mRNA was normalized using glyceraldehyde-3-phosphate dehydrogenase (GAPDH) as an endogenous control. The primer sequences were as follows: human CD47 (5′-GCTCTAAACAAGTC-CACTGTC-3′ and 5′-CATCTTCAAAGAGGCATCTCC-3′), and human GAPDH (5′-CCTCACAGTTGCCATGTAGA-3′ and 5′-TG GTACATGACAAGGTGCG-3′).

In vitro CD47-targeted NIR-PIT of BC cell lines

BC cell lines were removed from a culture flask using trypsin and incubated with phosphate-bufferED saline (PBS), anti-CD47, or anti-CD47-AF790. Then, cancer cells were seeded onto 96-well low-adhesion plates and irradiated with NIR (760–800 nm) light-emitting diode (Shanghai WinWorld Trading, SMO760). The light source was placed 0.2–0.3 cm above the cells and produced a light-power density of 100 mW/cm^2, which was measured with an optical power meter (Thorlabs, PM 100D). Cancer cells incubated with anti-CD47-AF790 received increasing light-energy levels of 0, 1, 4, 8, 16, or 32 J/cm^2, whereas cells incubated with anti-CD47 received 32 J/cm^2 or no irradiation. After 30 min of cell intervention, 10% of the cell suspension volume of propidium iodide (10 μg/mL) was added to each well of the 96-well plate and incubated at room temperature for 20 min followed by flow cytometry to detect the percentage of dead cells.

In vitro phagocytosis assay

Phagocytosis analysis was performed to evaluate the phagocytosis of anti-CD47-induced macrophages on cancer cells. RAW 264.7 macrophages were pre-cultured in a 15-mm laser confocal culture dish overnight. Three BC cell lines were removed from the culture flask using trypsin and incubated with PBS, IgG1-FITC, or anti-CD47-FITC, respectively. The cancer cells were added to the laser confocal culture dish, co-cultured with RAW 264.7 macrophages, and then observed by laser-scanning confocal microscopy.

The 5637 cells were removed from the culture flask using trypsin and incubated with PBS, anti-CD47, or anti-CD47-AF790, respectively. Cells were then seeded onto 96-well plates, in which RAW 264.7 macrophages were pre-cultured overnight. Cancer cells and macrophages were co-cultured and treated with 4 J/cm^2 NIR light intervention or no irradiation. Cell viability was measured by the CCK-8 method. Absorbance was detected at 450 nm by a microplate reader, and the data were analyzed using Thermo Scientific SkanIt.

Animal studies

Female Wistar rats (6 weeks old) and athymic NU/NU nude mice (4 weeks old) were purchased from Beijing Vital River Laboratory Animal Technology (Beijing, China). All animals were kept in pathogen-free and suitable temperature (25 ± 1°C) conditions with a light-dark cycle of 12/12 h. Water and standard diet were provided ad libitum, and the cages were changed twice weekly to maintain hygienic conditions. All procedures involving the animals were performed in accordance with the guidelines formulated by the Ethics Committee for Animal Experimentation of Shanxi Medical University (permission no. SYDL20200010).

Partial or complete tumor resection in xenograft mouse model

A total of 2×10^6 5637 cells in 50% Matrigel (Corning) were injected subcutaneously at the left forelimb pit of NU/NU nude mice. The calculation formula of tumor volume is (l × w^2)/2, where l = length and w = width. Tumor resection was performed when the volume reached ∼500 mm^3. For evaluation of CD47-targeted optical molecular imaging-assisted tumor resection and NIR-PIT *in vivo*, mice were randomly divided into six groups: A, B, C, D, E, and F, with eight mice in each group. Under the real-time guidance of optical molecular imaging mediated by ICG, 95% of the tumor in group A and group B was removed, and complete tumor resection was performed in group C. Under the real-time guidance of CD47-targeted optical molecular imaging, 95% of the tumor in groups D and E was removed, and complete tumor resection was performed in group F. Mice in group E received NIR light irradiation at an energy level of 100 J/cm^2 immediately and 24 h after surgery. ICG (2.5 mg/kg) or anti-CD47-AF790 (100 μg) was administered intravenously 24 h prior to tumor resection.

Before the wound was closed, two independent urologists were asked to distinguish which mice underwent complete tumor resection and which mice underwent partial tumor resection. Neither of them had prior knowledge about experimental design and surgical method. After sufficient hemostasis in the surgical area, the two urologists independently examined the wound and recorded the suspicious areas without any enhanced visual tools.

MicroCT scanning

In order to investigate the clinical value of routine imaging technology during surgery, microCT scanning (Bruker, Germany) was performed before wound closure to determine whether there was residual tumor in the wound and its location. Thirty representative animals (5 mice in each group) were imaged using the microCT before surgery, and then the mice were imaged again by utilizing the microCT after the tumor was partially or completely removed.

In vivo NIR-PIT of xenograft mouse model with tumor recurrence

Mice in groups A and B underwent partial tumor resection under the guidance of ICG-mediated optical molecular imaging, and the tumor recurrence was observed after surgery. When the tumor volume reached ∼100 mm^3, the therapeutic efficacy of repeated NIR-PIT in xenograft mouse model with tumor recurrence was evaluated. Mice

in group A served as the control group with no intervention. Mice in group B received NIR light irradiation at day 1 (100 J/cm^2) and day 2 (100 J/cm^2) after intravenous injection of 100 μg anti-CD47-AF790, once a week for 3 weeks.

Orthotopic rat model of BC

To induce the occurrence of space-occupying lesion in bladder, 30 female Wistar rats were given drinking water containing 0.05% N-butyl-N-(4-hydroxybutyl) nitrosamine (BBN; Tokyo Chemical Industry Japan). After 18 weeks, Wistar rats were imaged using a micro-MRI (Bruker, Germany) to detect whether a space-occupying lesion occurred in the bladder. Rats without a space-occupying lesion continued to be fed drinking water containing 0.05% BBN, and microMRI was performed once a week until a space-occupying lesion occurred.

***In vivo* optical molecular imaging in orthotopic rat model of BC**

Intravesical instillation of 2 μg of anti-CD47-AF790 was performed in rats with a -occupying lesion via the urethra through an angiocatheter 24-G intravenous indwelling needle plastic sheath (BD Bioscience). After 30 min, a small incision was made in the lower abdomen of the rat to expose the bladder. The bladder was cut longitudinally, and the entire bladder mucosa was imaged using the NIR imaging device. Under the guidance of CD47-targeted optical molecular imaging, the fluorescent sites in the bladder mucosa were marked. Then, the marked site and the suspicious malignant lesions visible by naked eye were removed. For each rat, if fewer than five specimens were removed through the above-mentioned steps, a random biopsy of bladder mucosa was needed to make the total number of specimens not fewer than five. The specimens were fixed in 4% paraformaldehyde and then embedded in paraffin for hematoxylin-eosin (HE) staining.

Statistical analysis

Qualitative statistics were expressed as numbers and percentages. For tumor recurrence rate, Fisher's exact test was used to compare the differences between two groups. Descriptive statistics were recorded as mean ± standard deviation. For CD47 mRNA expression level, *in vitro* NIR-PIT, and fluorescence intensity of tissue specimens, an unpaired t test was used to assess the differences between two groups. For phagocytosis of 5637 cells by macrophages and the tumor growth rate after repeated NIR-PIT, we used two-way ANOVA to evaluate the differences between control and experimental groups. Statistical analysis was performed using the statistical software GraphPad Prism, version 7.0 for Windows. Significant differences were reached when $p < 0.05$.

AVAILABILITY OF DATA AND MATERIALS

The datasets used and/or analyzed during the current study are available from the corresponding author on reasonable request.

ACKNOWLEDGMENTS

AUTHOR CONTRIBUTIONS

Y.J.Y. and X.F.Y. performed the conception and analyzed data. Y.J.Y., X.T.Y., J.W.L., and C.L. performed experiments and analyzed data. Y.J.Y., C.L., and X.F.Y. wrote, reviewed, and revised the manuscript.

DECLARATION OF INTEREST

The authors declare no competing interests.

REFERENCES

1. Babjuk, M., Burger, M., Compérat, E.M., Gontero, P., Mostafid, A.H., Palou, J., van Rhijn, B.W.G., Rouprêt, M., Shariat, S.F., Sylvester, R., et al. (2019). European association of urology guidelines on non-muscle-invasive bladder cancer (TaT1 and carcinoma in situ) - 2019 update. Eur. Urol. *76*, 639–657.

2. Cumberbatch, M.G.K., Foerster, B., Catto, J.W.F., Kamat, A.M., Kassouf, W., Jubber, I., Shariat, S.F., Sylvester, R.J., and Gontero, P. (2018). Repeat transurethral resection in non-muscle-invasive bladder cancer: a systematic review. Eur. Urol. *73*, 925–933.

3. Ritch, C.R., Velasquez, M.C., Kwon, D., Becerra, M.F., Soodana-Prakash, N., Atluri, V.S., Almengo, K., Alameddine, M., Kineish, O., Kava, B.R., et al. (2020). Use and validation of the AUA/SUO risk grouping for nonmuscle invasive bladder cancer in a contemporary cohort. J. Urol. *203*, 505–511.

4. Lenis, A.T., Lec, P.M., Chamie, K., and Mshs, M.D. (2020). Bladder cancer: a review. JAMA *324*, 1980–1991.

5. Witjes, J.A., Bruins, H.M., Cathomas, R., Compérat, E.M., Cowan, N.C., Gakis, G., Hernández, V., Linares Espinós, E., Lorch, A., Neuzillet, Y., et al. (2021). European association of urology guidelines on muscle-invasive and metastatic bladder cancer: summary of the 2020 guidelines. Eur. Urol. *79*, 82–104.

6. Sloan, F.A., Yashkin, A.P., Akushevich, I., and Inman, B.A. (2020). The cost to medicare of bladder cancer care. Eur. Urol. Oncol. *3*, 515–522.

7. Tan, W.S., Teo, C.H., Chan, D., Ang, K.M., Heinrich, M., Feber, A., Sarpong, R., Williams, N., Brew-Graves, C., Ng, C.J., et al. (2020). Exploring patients' experience and perception of being diagnosed with bladder cancer: a mixed-methods approach. BJU Int. *125*, 669–678.

8. Chou, R., Selph, S., Buckley, D.I., Fu, R., Griffin, J.C., Grusing, S., and Gore, J.L. (2017). Comparative effectiveness of fluorescent versus white light cystoscopy for initial diagnosis or surveillance of bladder cancer on clinical outcomes: systematic review and meta-analysis. J. Urol. *197*, 548–558.

9. Naito, S., Algaba, F., Babjuk, M., Bryan, R.T., Sun, Y.H., Valiquette, L., and de la Rosette, J.; CROES Narrow Band Imaging Global Study Group (2016). The clinical research office of the endourological society (CROES) multicentre randomised trial of narrow band imaging-assisted transurethral resection of bladder tumour (TURBT) versus conventional white light imaging-assisted TURBT in primary non-muscle-invasive bladder cancer patients: trial protocol and 1-year results. Eur. Urol. *70*, 506–515.

10. Chen, C., Huang, H., Zhao, Y., Liu, H., Luo, Y., Sylvester, R.J., Li, J.P., Lam, T.B., Lin, T., and Huang, J. (2020). Diagnostic accuracy of photodynamic diagnosis with 5-aminolevulinic acid, hexaminolevulinate and narrow band imaging for non-muscle invasive bladder cancer. J. Cancer *11*, 1082–1093.

11. Hernot, S., van Manen, L., Debie, P., Mieog, J.S.D., and Vahrmeijer, A.L. (2019). Latest developments in molecular tracers for fluorescence image-guided cancer surgery. Lancet Oncol. *20*, e354–e367.

12. Chan, K.S., Espinosa, I., Chao, M., Wong, D., Ailles, L., Diehn, M., Gill, H., Presti, J., Jr., Chang, H.Y., van de Rijn, M., et al. (2009). Identification, molecular

characterization, clinical prognosis, and therapeutic targeting of human bladder tumor-initiating cells. Proc. Natl. Acad. Sci. U S A *106*, 14016–14021.

13. Logtenberg, M.E.W., Scheeren, F.A., and Schumacher, T.N. (2020). The CD47-SIRPα immune checkpoint. Immunity *52*, 742–752.

14. Pan, Y., Volkmer, J.P., Mach, K.E., Rouse, R.V., Liu, J.J., Sahoo, D., Chang, T.C., Metzner, T.J., Kang, L., van de Rijn, M., et al. (2014). Endoscopic molecular imaging of human bladder cancer using a CD47 antibody. Sci. Transl. Med. *6*, 260ra148.

15. Ansell, S.M., Maris, M., Lesokhin, A.M., Chen, R., Flinn, I.W., Sawas, A., Minden, M.D., Villa, D., Percival, M.M., Advani, A.S., et al. (2021). Phase 1 study of the CD47 blocker TTI-621 in patients with relapsed or refractory hematologic malignancies. Clin. Cancer Res. *27*, 2190–2199.

16. Sikic, B.I., Lakhani, N., Patnaik, A., Shah, S.A., Chandana, S.R., Rasco, D., Colevas, A.D., O'Rourke, T., Narayanan, S., Papadopoulos, K., et al. (2019). First-in-human, first-in-class phase I trial of the anti-CD47 antibody Hu5F9-G4 in patients with advanced cancers. J. Clin. Oncol. *37*, 946–953.

17. Jensen, M.M., Jørgensen, J.T., Binderup, T., and Kjaer, A. (2008). Tumor volume in subcutaneous mouse xenografts measured by microCT is more accurate and reproducible than determined by 18F-FDG-microPET or external caliper. BMC Med. Imaging *8*, 16.

18. Debie, P., and Hernot, S. (2019). Emerging fluorescent molecular tracers to guide intra-operative surgical decision-making. Front. Pharmacol. *10*, 510.

19. Yang, Y., Yang, X., Liu, C., and Li, J. (2020). Preliminary study on the application of en bloc resection combined with near-infrared molecular imaging technique in the diagnosis and treatment of bladder cancer. World J. Urol. *38*, 3169–3176.

20. Wang, J., Fang, R., Wang, L., Chen, G., Wang, H., Wang, Z., Zhao, D., Pavlov, V.N., Kabirov, I., Wang, Z., et al. (2018). Identification of carbonic anhydrase IX as a novel target for endoscopic molecular imaging of human bladder cancer. Cell. Physiol. Biochem. *47*, 1565–1577.

21. Kiss, B., van den Berg, N.S., Ertsey, R., McKenna, K., Mach, K.E., Zhang, C.A., Volkmer, J.P., Weissman, I.L., Rosenthal, E.L., and Liao, J.C. (2019). CD47-targeted near-infrared photoimmunotherapy for human bladder cancer. Clin. Cancer Res. *25*, 3561–3571.

22. Railkar, R., Krane, L.S., Li, Q.Q., Sanford, T., Siddiqui, M.R., Haines, D., Vourganti, S., Brancato, S.J., Choyke, P.L., Kobayashi, H., et al. (2017). Epidermal growth factor receptor (EGFR)-targeted photoimmunotherapy (PIT) for the treatment of EGFR-expressing bladder cancer. Mol. Cancer Ther. *16*, 2201–2214.

23. Siddiqui, M.R., Railkar, R., Sanford, T., Crooks, D.R., Eckhaus, M.A., Haines, D., Choyke, P.L., Kobayashi, H., and Agarwal, P.K. (2019). Targeting epidermal growth factor receptor (EGFR) and human epidermal growth factor receptor 2 (HER2) expressing bladder cancer using combination photoimmunotherapy (PIT). Sci. Rep. *9*, 2084.

24. Lee, S.M., Lee, E.J., Hong, H.Y., Kwon, M.K., Kwon, T.H., Choi, J.Y., Park, R.W., Kwon, T.G., Yoo, E.S., Yoon, G.S., et al. (2007). Targeting bladder tumor cells in vivo and in the urine with a peptide identified by phage display. Mol. Cancer Res. *5*, 11–19.

25. Yang, X., Zhang, F., Luo, J., Pang, J., Yan, S., Luo, F., Liu, J., Wang, W., Cui, Y., and Su, X. (2016). A new non-muscle-invasive bladder tumor-homing peptide identified by phage display in vivo. Oncol. Rep. *36*, 79–89.

26. Peng, L., Shang, W., Guo, P., He, K., Wang, H., Han, Z., Jiang, H., Tian, J., Wang, K., and Xu, W. (2018). Phage display-derived peptide-based dual-modality imaging probe for bladder cancer diagnosis and resection postinstillation: a preclinical study. Mol. Cancer Ther. *17*, 2100–2111.

27. Zhang, H., Aina, O.H., Lam, K.S., de Vere White, R., Evans, C., Henderson, P., Lara, P.N., Wang, X., Bassuk, J.A., and Pan, C.X. (2012). Identification of a bladder cancer-specific ligand using a combinatorial chemistry approach. Urol. Oncol. *30*, 635–645.

28. Golijanin, J., Amin, A., Moshnikova, A., Brito, J.M., Tran, T.Y., Adochite, R.C., Andreev, G.O., Crawford, T., Engelman, D.M., Andreev, O.A., et al. (2016). Targeted imaging of urothelium carcinoma in human bladders by an ICG pHLIP peptide ex vivo. Proc. Natl. Acad. Sci. U S A *113*, 11829–11834.

29. Chaux, A., Cohen, J.S., Schultz, L., Albadine, R., Jadallah, S., Murphy, K.M., Sharma, R., Schoenberg, M.P., and Netto, G.J. (2012). High epidermal growth factor receptor immunohistochemical expression in urothelial carcinoma of the bladder is not associated with EGFR mutations in exons 19 and 21: a study using formalin-fixed, paraffin-embedded archival tissues. Hum. Pathol. *43*, 1590–1595.

30. Røtterud, R., Nesland, J.M., Berner, A., and Fosså, S.D. (2005). Expression of the epidermal growth factor receptor family in normal and malignant urothelium. BJU Int. *95*, 1344–1350.

31. Cancer Genome Atlas Research Network (2014). Comprehensive molecular characterization of urothelial bladder carcinoma. Nature *507*, 315–322.

32. Klatte, T., Seligson, D.B., Rao, J.Y., Yu, H., de Martino, M., Kawaoka, K., Wong, S.G., Belldegrun, A.S., and Pantuck, A.J. (2009). Carbonic anhydrase IX in bladder cancer: a diagnostic, prognostic, and therapeutic molecular marker. Cancer *115*, 1448–1458.

33. de Martino, M., Lucca, I., Mbeutcha, A., Wiener, H.G., Haitel, A., Susani, M., Shariat, S.F., and Klatte, T. (2015). Carbonic anhydrase IX as a diagnostic urinary marker for urothelial bladder cancer. Eur. Urol. *68*, 552–554.

34. Guzzo, T.J., Magheli, A., Bivalacqua, T.J., Nielsen, M.E., Attenello, F.J., Schoenberg, M.P., and Gonzalgo, M.L. (2009). Pathological upstaging during radical cystectomy is associated with worse recurrence-free survival in patients with Bacillus Calmette-Guerin-refractory bladder cancer. Urology *74*, 1276–1280.

35. Liu, J.J., Droller, M.J., and Liao, J.C. (2012). New optical imaging technologies for bladder cancer: considerations and perspectives. J. Urol. *188*, 361–368. https://doi.org/10.1016/j.juro.2012.03.127.

36. Liem, E.I.M.L., Freund, J.E., Savci-Heijink, C.D., de la Rosette, J.J.M.C.H., Kamphuis, G.M., Baard, J., Liao, J.C., van Leeuwen, T.G., de Reijke, T.M., and de Bruin, D.M. (2020). Validation of confocal laser endomicroscopy features of bladder cancer: the next step towards real-time histologic grading. Eur. Urol. Focus 6, 81–87.

37. Xiong, Y.Q., Tan, J., Liu, Y.M., Li, Y.Z., You, F.F., Zhang, M.Y., Chen, Q., Zou, K., and Sun, X. (2019). Diagnostic accuracy of optical coherence tomography for bladder cancer: a systematic review and meta-analysis. Photodiagnosis Photodyn Ther. *27*, 298–304.

38. Kiss, B., Marcq, G., and Liao, J.C. (2018). Optical and cross-sectional imaging technologies for bladder cancer. Cancer Treat. Res. *175*, 139–163.

39. Madajewski, B., Judy, B.F., Mouchli, A., Kapoor, V., Holt, D., Wang, M.D., Nie, S., and Singhal, S. (2012). Intraoperative near-infrared imaging of surgical wounds after tumor resections can detect residual disease. Clin. Cancer Res. *18*, 5741–5751.

40. Earl, J., Rico, D., Carrillo-de-Santa-Pau, E., Rodríguez-Santiago, B., Méndez-Pertuz, M., Auer, H., Gómez, G., Grossman, H.B., Pisano, D.G., Schulz, W.A., et al. (2015). The UBC-40 urothelial bladder cancer cell line index: a genomic resource for functional studies. BMC Genomics *16*, 403.